





Impact of Irradiance Data on the Energy Yield Modeling of Dual-Junction Solar Module Stacks for One-Sun Applications

Oliver Höhn , Jayanth N. Murthy , Marc Steiner, Nico Tucher, Elke Lorenz, Jan Christoph Goldschmidt , Frank Dimroth , *Member, IEEE*, and Benedikt Bläsi

Abstract—With silicon-based tandem solar cells nearing commercialization, the significance of predicting the outdoor performance of tandem solar devices is growing. Although several models exist to calculate the outdoor performance, the availability of high-resolution irradiance data is limited. Therefore, we study the influence of the resolution of the irradiance data on the predicted energy yield of a 2-terminal III-V/Si tandem device. As an exemplary location, Golden, CO, USA, was chosen. We found that a wavelength resolution as low as 50 nm leads to a deviation of only 0.2% relative. We especially found that satellite-derived spectral data that are split into Kato bands lead to a deviation of 0.7% relative for Golden, CO, and, thus, are sufficient to model the energy yield of tandem devices. Confirming this finding for further locations has to be the scope of future work.

Index Terms—Energy yield, multijunction solar cells, photovoltaics, silicon-based tandem solar cells.

I. INTRODUCTION

SOLAR cells and photovoltaic (PV) systems have advanced remarkably in the past few decades. In 2019 alone, 90% of globally installed PV systems were based on crystalline silicon [1]. However, silicon solar cells have an intrinsic efficiency limit of 29.4% [2], which current cell technologies are approaching fast. One possibility to overcome this limit is provided by silicon-based tandem solar cells [3]. With the aim of increasing the conversion efficiency to more than 30%, a number of new cell architectures incorporating silicon as the bottom cell are investigated. Strategies to form these cells consider a wide-bandgap top cell in the form of a-Si [4], Perovskite [5], III-V solar cells

[6], or nanowires [7]. The bandgap combination of the materials is important for the optimization of the power produced by a tandem solar device. Using the Shockley–Queisser detailed balance method with the AM1.5G spectrum yields an optimum bandgap combination for a silicon-based dual-junction device of 1.1 and 1.72 eV. Based on those values, idealized efficiencies up to 45% are predicted [8]. Adapting the idealized model to realistic conditions needs to take into account the material quality (electrical/optical properties) and the resulting dependencies of the optimum band gaps. Furthermore, outdoor irradiation conditions in comparison to the AM1.5G spectrum can strongly influence the solar cell performance [9]–[12].

Compared with a 4-terminal (4T) tandem solar cell, a 2-terminal (2T) configuration has the advantage of lower parasitic absorption [13] and less electrical wiring at module level.

However, a 2T tandem device design needs to minimize current-mismatch losses [14]. As a result, there is a strong interest to get to know the outdoor energy yield instead of the standard testing conditions (STC) efficiency. This is particularly true for tandem devices. Such an analysis of the energy yield is crucial in determining the potential and the electricity costs of new and emerging PV technologies in varying configurations.

There are various models that describe the process of calculating energy yield [14]–[27]. However, realistic outdoor spectral data as central input parameter for a yield calculation are difficult to obtain if a high wavelength resolution is required. Measurement-based outdoor spectra are limited to very few locations in the world, particularly set up by research labs. They are also limited in the continuous availability of the recordings. Satellite-derived spectral data can be obtained for any location in the world, and many decades of data can be utilized, but they are limited in their accuracy.

In this article, we investigate if such low-resolution spectral datasets are sufficient to calculate accurate power yields for silicon-based tandem solar cells. Because of the availability of highly accurate and sufficiently broad spectral data, the energy yield is exemplarily calculated for Golden, CO, USA.

The spectral resolution as well as the time resolution is changed, and the energy yield is calculated and compared with the energy yield of the fully resolved spectrum. Additionally, the effect of the availability of direct and diffuse spectral data

Manuscript received November 5, 2020; revised December 21, 2020; accepted March 1, 2021. Date of publication March 29, 2021; date of current version April 21, 2021. This work was supported in part by the European Union's Horizon 2020 Research and Innovation Program within the Project SiTaSol under Grant 727497 and in part by the German Research Foundation (DFG) through the project Oposit. (*Corresponding author: Oliver Höhn.*)

The authors are with the Fraunhofer Institute for Solar Energy Systems, 79110 Freiburg, Germany (e-mail: oliver.hoehn@ise.fraunhofer.de; jayanth.n.murthy@gmail.com; marc.steiner@ise.fraunhofer.de; nico.tucher@ise.fraunhofer.de; elke.lorenz@ise.fraunhofer.de; jan.christoph.goldschmidt@ise.fraunhofer.de; frank.dimroth@ise.fraunhofer.de; benedikt.blaesi@ise.fraunhofer.de).

Color versions of one or more figures in this article are available at <https://doi.org/10.1109/JPHOTOV.2021.3064562>.

Digital Object Identifier 10.1109/JPHOTOV.2021.3064562

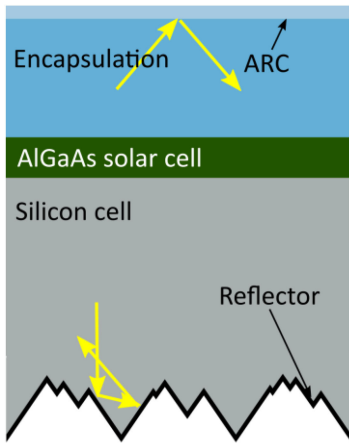


Fig. 1. Sketch of the simulated module stack. At the rear side, random pyramids in combination with a silver mirror are assumed for light trapping.

as compared with only using global spectral data and direct and diffuse irradiance is investigated.

As exemplary system, an AlGaAs top solar cell with a band gap of 1.7 eV is assumed. As bottom solar cell a silicon solar cell is supposed. The modeling is performed on a module stack (see Fig. 1)

In a final step, satellite-based data [28], [29] from the same location are used to calculate the energy yield, which is compared with the results from ground-measured data.

The presented method is a path to understand the requirements and suitability of spectral data, when estimating the energy yield of silicon-based tandem solar cells. If sufficiently precise yield analyses are possible based on low-resolution spectra, this will strongly facilitate all further modeling.

II. ENERGY YIELD MODELING SCHEME

The model to determine the energy yield of tandem solar modules requires the following input parameters.

- 1) Meteorological data for the location under study, including timewise spectral irradiance I and ambient temperature T_{amb} .
- 2) Electrical parameters of the solar module technology required to generate current–voltage curves for different photocurrents J_{ph} , at different module temperatures, using the two-diode model.
- 3) The external quantum efficiency (EQE), that is resolved with respect to wavelength λ , angle of incidence of irradiance on the module plane, and temperature of the module T .

Within this study, we assume the following empirical relation between T_{amb} and T as given by [30]

$$T = (\bar{I}/1000) \cdot 25 + T_{\text{amb}} \quad (1)$$

where \bar{I} is the absolute value of the global irradiance power on the module plane.

A. Irradiance Data

The required wavelength and angular resolved spectral irradiance data can be generated in different ways. In this work the investigated sources are as follows.

- 1) Measured irradiance data using ground-measurement instruments such as NREL’s Baseline Measurement System (BMS) located in Golden, Colorado, USA [35].
- 2) Modeled irradiance data using atmospheric data from geostationary satellites [31]–[33] that:
 - lowerLetter%1) consist of spectral data within specific wavelength bands, such as “Kato bands” [34];
 - lowerLetter%1) only contain global spectral data and direct and diffuse irradiance [28], [29].

Relevant differences between the spectral data from ground-measured data and satellite-based data are: 1) the wavelength; 2) time resolution; and 3) whether direct and diffuse spectra are separated. Ground-based tools can give resolutions of a few nanometers and in the range of a few minutes in combination with a separation into direct and diffuse spectral data. Satellite-based data are often derived in so-called Kato bands. Kato bands are constructed with the idea that various atmospheric parameters tend to affect the irradiation spectra in different wavelength regions. This results in the construction of a spectrum having nonuniform wavelength bands, whose accuracy depends on the accuracy of the atmospheric parameters used for its construction [32], [36], [37]. Using Kato bands, the spectral data can also be split into direct and diffuse irradiance.

A second option for satellite data is to have a high resolution, but to only give global spectra and direct and diffuse irradiance.

In this article, ground-measured spectral data for Golden, CO, USA, are used. The spectral resolution is varied—especially, a Kato band resolution is generated to test if such spectra are suitable for the calculation of an energy yield of silicon-based tandem solar cells.

In a final step, the results from ground-measured data are compared with results from satellite-based data [28], [29]. Note that the satellite-based data in this case have high spectral resolution but contain only the global spectrum and diffuse and direct irradiance. In other words, for diffuse and direct components, the same spectrum, but different irradiance, is used.

B. Temperature Dependent Current–Voltage Curves

There are very different models to describe the electrical behavior of solar cells. A 2-diode model, including series and parallel resistances R_s and R_p , is used in this work for each of the junctions. The 2-diode models for each junction are, in the end, interconnected in series to account for the chosen 2T configuration [38]. This model is chosen as it is simple but can describe the IV-characteristics of the silicon bottom and the III-V top cell accurately in order to model the energy yield.

The following implicit equation for current density of a single-junction solar cell J_{junction} , at a particular voltage V_{junction} , that includes dark saturation current densities J_{01} , J_{02} [39], is

TABLE I
ELECTRICAL PARAMETERS AT 298K FOR THE DEVICES USED IN THIS WORK

Parameter	Symbol	Units	Silicon (bottom) cell		AlGaAs top cell	
			[53]		[50, 54]	
Material bandgap	E_g	eV	1.11		1.70	
Series resistance	R_s	$\Omega \cdot \text{cm}^2$	0.1035		0.1030	
Parallel resistance	R_p	$\Omega \cdot \text{cm}^2$	5e3		10e3	
Saturation current density	J_{01}	mA/cm^2	2.28e-11	A_{01}	$\text{mA}/\text{cm}^2/\text{K}^3$	0.088
				B_{01}	eV^{-1}	1.625
	J_{02}	mA/cm^2	7.66e-07	β_{02}	$\text{mA}/\text{cm}^2/\text{K}^{2.5}$	0.040

calculated as follows:

$$\begin{aligned}
 J_{\text{junction}}(V_{\text{junction}}) = & \\
 & J_{ph} - J_{01}(T) \left[\exp\left(\frac{q(V_{\text{junction}} + R_s \cdot J)}{n_1 k_B T}\right) - 1 \right] \\
 & - J_{02}(T) \left[\exp\left(\frac{q(V_{\text{junction}} + R_s \cdot J)}{n_2 k_B T}\right) - 1 \right] \\
 & + \left(\frac{V_{\text{junction}} + R_s \cdot J_{\text{junction}}}{R_p} \right) \quad (2)
 \end{aligned}$$

where J_{ph} is the photocurrent density, q is the elementary charge, $n_1 = 1$ and $n_2 = 2$ are the ideality factors for J_{01} and J_{02} respectively, and k_B is the Boltzmann constant.

Temperature-dependent parameters for the bandgap variation of Si are taken from Singh *et al.* [40]. For the III-V top cell, J_{01} and its dependence on temperature follow the Wanlass model, as shown in [41]

$$J_{01}(T) = \beta_{01}(T) T^3 \exp\left(-\frac{E_g(T)}{k_B T}\right) \quad (3)$$

where the pre-exponential factor β , and the bandgap of the junction E_g , are dependent on temperature, and β_{01} can be modeled as [42]

$$\beta_{01}(T) = A_{01} \cdot \exp(B_{01} \cdot E_g(T)) \quad (4)$$

where $A_{01} = 0.0269 \text{ Am}^{-2}\text{K}^{-3}$ and $B_{01} = 1.6252 \text{ eV}^{-1}$ represent the radiative limit on account of fitting the Wanlass model to the detailed balance radiative limit [42], [43]. The saturation current density for the III-V top cell J_{02} is expressed as [44]

$$J_{02}(T) = \beta_{02} T^{2.5} \exp\left(-\frac{E_g(T)}{k_B T}\right). \quad (5)$$

The molar fraction-dependent bandgap of the solar cell materials is computed for $\text{Al}_x\text{Ga}_{(1-x)}\text{As}$ using material parameters for tertiary III-V compounds adopted from [45]. The Varshni relation [46] is used to model the bandgap dependence on temperature. Subsequently, optical data for $\text{Al}_x\text{Ga}_{(1-x)}\text{As}$ are corrected for temperature dependence using a bandgap shift model [47]. The parameters for the silicon single-junction reference device and silicon junction of the dual-junction device are based on the n-type Si cell in [48]. The electrical parameters for the AlGaAs junction with varying composition are based

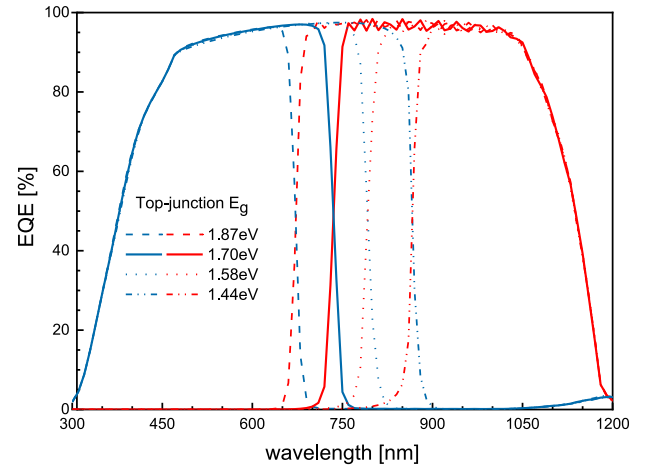


Fig. 2. Wavelength-resolved EQEs for different top-junction bandgap configurations of the tandem solar module, at a module temperature of 298 K and normal incidence. EQEs are calculated using OPTOS.

on Wanlass parameters found for GaAs in [49] and adopted for $\text{Al}_{0.19}\text{Ga}_{0.81}\text{As}$ from [45]. Table I lists the electrical parameters at 298 K for both devices used in this work.

C. Spectral Response of Solar Modules (EQE)

The optical performance of the solar devices considered in this article is modeled with the matrix-based simulation formalism, OPTOS [50], [51]. With this formalism, absorptance, reflectance, and transmittance of the incident light across individual layers of the solar cell can be obtained [52]. The obtained absorptance can be regarded as an optimum EQE under the assumption that all photogenerated carriers are collected and contribute to the photocurrent (see Fig. 2). The temperature dependence of the EQE is obtained using a bandgap shift model [47]. Temperature dependence of the bandgap is modeled using the Varshni relation [46], and parameters obtained from [45] for III-V materials.

The EQE results obtained from OPTOS are for a large number of discrete incidence angles of direct irradiance within the angular space surrounding the solar module surface. The modeling of spectral response for diffuse irradiance, however, must include all possible angles of incidence of the diffuse light upon the module surface [52].

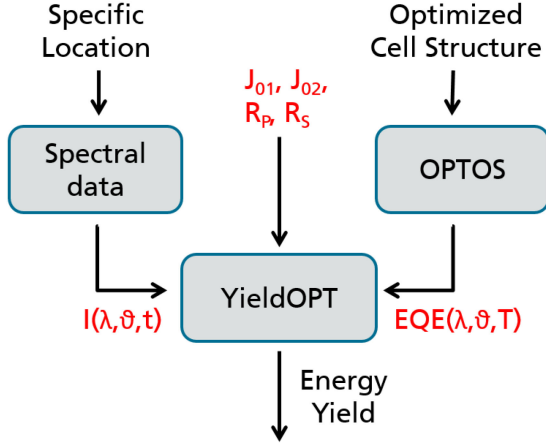


Fig. 3. Sketch summarizing the various components of the energy yield model described in this work [22].

The diffuse component of global irradiance consists of light from all incidence angles θ , which is complex to calculate. For the sake of simplicity, the sky is assumed to be isotropic [53]. The EQEs corresponding to direct light are used to calculate the diffuse spectral response by weighting with the solid angle Ω

$$EQ E_{diffuse} = \frac{\int EQE(\theta, T) \cos(\theta) d\Omega}{\int \cos(\theta) d\Omega}. \quad (6)$$

Individual EQEs obtained from OPTOS are available for a discrete number of angle channels, and hence, are weighted over their corresponding angles of incidence under the summation represented by the following equation:

$$EQ E_{diffuse} = \frac{\sum EQE(\theta, T) \cos(\theta) \sin(\theta)}{\sum \cos(\theta) \sin(\theta)}. \quad (7)$$

Combined Model: Fig. 3 summarizes all the input parameters needed for the energy yield model, namely, spectral data that are either obtained from measurement devices or retrieved from satellite models, electrical parameters of the solar module and its individual subcells, and the optically modeled EQEs are used within YieldOpt [19]. Its usage to obtain monthly and annual results was successfully demonstrated by Tucher *et al.* [22]. This model also takes into account the orientation and tilt of the device surface.

III. RESULTS AND DISCUSSION

A. Effect of Resolution

1) **Wavelength Resolution:** As the reference dataset for this study, annual spectral data obtained from measurement sites in Golden, CO, for the year of 2018 are chosen. The dataset includes global horizontal irradiance (GHI WISER) and the direct normal irradiance (DNI PGS100) with wavelength resolutions of 1 and 0.7 nm, respectively [35].

These measurement data represent the actual sky conditions at the location and is available every 5 min of the year. To study the effect of wavelength resolution on the calculated energy yield, datasets with lower wavelength resolution are derived from the

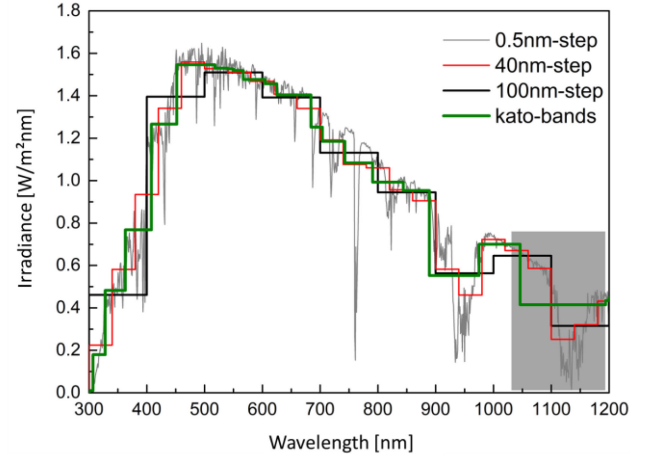


Fig. 4. Exemplary spectra with uniform wavelength steps (40, 100 nm) and Kato bands in comparison with a full resolution irradiance spectra (0.5 nm), within a wavelength range of (300–1200 nm) considered for the spectral response of the solar modules. Observe the peculiarly large wavelength step of the Kato band spectrum around 1050–1200 nm (band 23).

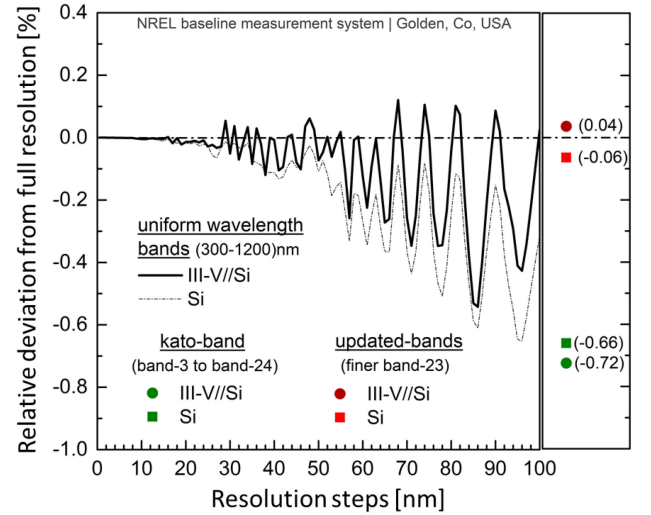


Fig. 5. Relative deviation of annual energy yield of the tandem device as well as the single-junction Si device, with irradiance spectra in uniform wavelength bands varied between 1 to 100 nm (left) and Kato bands (right) with respect to full resolution irradiance spectra. The updated bands have three smaller wavelength bands in place of the larger Kato band number 23.

original datasets, with uniform wavelength resolution steps in the range of 1–100 nm. These derived datasets ensure energy conservation in relation to the original dataset.

From these derived datasets, nonuniform wavelength resolutions, i.e., the varying wavelength bands listed in Table II, also called Kato bands [34], were derived. As stated above, those Kato bands can be derived from satellite-based spectral data and are created artificially from higher resolution data here.

Fig. 4 shows exemplary spectra for each of the derived datasets with uniform wavelength interval (40 and 100 nm steps) and that of the Kato bands, in comparison to the full resolution reference dataset (0.5 nm step).

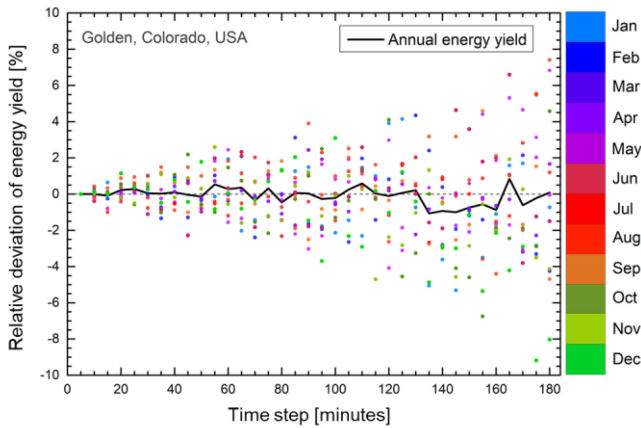


Fig. 6. Relative deviation of energy yield at Golden, CO, with respect to the temporal resolution of irradiance dataset. For every time-step, the colored points represent monthly energy yield. The black line indicates annual energy yield.

The resulting annual energy yield data obtained for each of these wavelength-resolution-sets were calculated for the above described dual-junction module stack and the single-junction Si module stack. The devices are oriented with a 40° tilt facing south that corresponds to the latitude of the location in the northern hemisphere. The results are plotted against their respective wavelength resolution steps in Fig. 5.

The energy yield results obtained for wavelength resolutions of up to 25 nm agree with the reference and do not change much. This is a very important result as it shows that for the yield analysis of the tandem cells within this work, a wavelength resolution of 25 nm is sufficient. This resolution can be provided by many datasets throughout the world and makes high-resolution measurements unnecessary for the analysis. However, the maximum deviation of energy yield calculated in comparison to the full resolution dataset within this wavelength range is about 0.7% relative. The oscillations observed are a result of the step-nature of the lower resolution spectra in combination with the steep changes in irradiance intensity and in the EQE of the solar module in the range of 300–400 nm and toward longer wavelengths around (1000–1200) nm.

A further conclusion from the results in Fig. 6 is that the Kato band spectral dataset produces the highest deviation in calculated annual energy yield.

This is almost completely because of band number 23 that has a width of 148 nm, larger than the width of the sudden dip in the irradiation spectrum within this region caused because of water vapor absorption (see Fig. 4 grey box). Already splitting band 23 into three bands ([1046–1110] nm, [1110–1165] nm, and [1165–1194] nm), would reduce the deviation of the energy yield calculated from such a dataset to below 0.1%, from the previously observed 0.7% for the actual Kato bands. Note that a similar decrease in difference can also be reached by only creating two bands out of band 23. The main point is that the mentioned Kato band does not fit to the band gap of the silicon bottom solar cell.

2) *Temporal Resolution*: The time interval between consecutive sets of measurements available within a dataset is called

its temporal resolution. Measurement datasets recorded by spectroradiometers at Golden, CO, in the year 2018, have a temporal resolution of 5 min.

Time-steps from 5 to 180 min in steps of 5 min are filtered for each day starting from sunrise, e.g., for the 20-min resolution, only the datasets every 20 min was extracted. The datasets with other time-steps in between were, in this case, ignored.

Monthly and annual energy yield is calculated for the reduced temporal resolution, and is compared with that of the full resolution dataset, as shown in Fig. 6. It is observed that on the annual scale, the seasonal overestimations and underestimations compensate each other, resulting in a deviation that is less than 0.5 % relative for a temporal resolution below 100 min, and within 1 % until 180 min. This is again an important finding for further yield analyses, as spectral data with a temporal resolution of 1 h are often found in satellite-based data, while higher resolution data are sparse.

For monthly energy yield, deviation is less than 3% for temporal resolutions up to 80 min. However, in order to calculate energy yields for shorter time scales, less than a month, a very high temporal resolution, having time-steps of a few minutes, is essential. Such high resolutions are also required in order to account for the impact of cloud transient effects, thereby increasing the accuracy of energy yield prediction [54]–[56].

3) *Availability of Direct and Diffuse Spectra*: Finally, the yield calculation was performed using only the global spectrum for direct as well as diffuse light. The spectrum is scaled to the direct and diffuse irradiance, respectively. This simulates the case that diffuse and direct irradiance data is available, but only the global spectra, which is, e.g., the case for the satellite-based dataset used in this work. We found no difference in energy yield, for a silicon single-junction solar cell, when only using the global spectrum as compared with the full spectral split. However, for the tandem device, the energy yield was underestimated by 0.7% in this case.

B. Comparison of Satellite-Based and Ground Measured Data

Up to this point, the analysis was purely based on ground-measured data from Golden, CO, USA. As a final step in this analysis, the results from the energy yield of the ground-measured data and satellite-based data (see Section II-A) are compared. The satellite-based data in this case have a high spectral resolution, but only a global spectrum with direct and diffuse irradiation. The STC efficiency of the silicon single-junction device is 26.3% and of the AlGaAs/Si dual-junction device is 35.6%, respectively. The results for the energy yield calculation can be found in Tables II and III.

The annual irradiation differs by 1.8% relative between ground-measured and satellite-based data, which is an excellent agreement. The harvesting efficiency is underestimated by 0.4% for the silicon single-junction device and by 0.5% for the AlGaAs/Si dual-junction device. From the analysis before, we expected an underestimation of the energy yield of 0.7%, when not using separate spectra for direct and diffuse light. This good agreement allows for the use of satellite-based data for the estimation of energy yield of silicon-based dual-junction solar cells.

TABLE II
COMPARISON OF THE PERFORMANCE FOR THE ALGAAS/SI-DUAL-JUNCTION DEVICE USED IN THIS WORK USING GROUND MEASURED DATA AND SATELLITE-BASED DATA

Parameter	Units	Ground Measured	Satellite Based	Relative Difference
Total annual irradiation 40° fixed tilt, S-facing plane (Golden, Co, 2018)	kWh/ m ²	1980	2017	1.8%
Energy yield 40° fixed tilt, S-facing plane	kWh/ m ²	648	657	1.3%
Harvesting efficiency	%	32.72	32.57	-0.5%

TABLE III
COMPARISON OF THE PERFORMANCE FOR THE SI-SJ DEVICE USED IN THIS WORK USING GROUND MEASURED DATA AND SATELLITE-BASED DATA

Parameter	Units	Ground Measured	Satellite Based	Relative Difference
Total annual irradiation 40° fixed tilt, S-facing plane (Golden, Co, 2018)	kWh/ m ²	1980	2017	1.8%
Energy yield 40° fixed tilt, S-facing plane	kWh/ m ²	488	495	1.4%
Harvesting efficiency	%	24.64	24.54	-0.4%

C. Discussion

Overall satellite-based data either with Kato bands with a split into direct and diffuse spectrum or data with high spectral resolution, but only a split of direct and diffuse irradiance lead to a difference below 1% relative in energy yield. Note that the difference in harvesting efficiency for the single and the dual junction is similar when comparing satellite-based datasets to ground-measured data.

Thus, these types of satellite-based spectra can, in principle, be used to accurately model the energy yield of silicon-based dual-junction solar cells. Note that this conclusion is only based on one location and one specific device and should be confirmed for other devices and locations, for a general validation in future work.

IV. CONCLUSION

We presented an approach to determine the energy yield of tandem solar devices.

The impact of different spectral components on the accuracy of the energy yield of a III-V on silicon dual-junction solar cell was determined, using annual spectral data for Golden, CO, USA. Wavelength resolution steps of up to 50 nm showed a deviation of less than 0.2%_{rel} in the energy yield calculation, under the condition that the corresponding energy of the lower resolution irradiation spectra is conserved. A deviation of less than 0.5%_{rel} was found for a time resolution of up to 100 min. It was especially shown that spectra split into Kato bands, which can be derived from satellite-based data, and can be used with a deviation of 0.7% for PV applications.

Data that only contain global spectrum but direct and diffuse irradiance lead to the same deviation of 0.7%.

Finally, a comparison between real satellite-based data and the ground-measured data resulted in a difference of 0.5% in yield, which perfectly fits to the expected 0.7% difference. The difference in irradiation of the used satellite-based data and the ground-measured data is 1.8%. Having in mind the large number of assumptions that lead to these results, this agreement is also very good.

Currently, the main aim of yield analyses for silicon-based tandem solar cells is technology comparison, especially a comparison to silicon single-junction devices. As the expected gain in performance is in the range of 20%_{rel}, a maximum error of a few percent relative does not influence the outcome in a relevant manner and, thus, is sufficiently small. Based on these results, satellite-based spectral data can be used to estimate the energy yield of silicon-based tandem solar cells.

However, confirming this finding for further locations with the presented method has to be the scope of future work in order to finally prove the usability of low-resolution spectra for the yield estimation of silicon-based tandem devices for one-sun applications.

REFERENCES

- [1] S. Philipps and W. Warmuth, "Photovoltaics report—Fraunhofer Institute for Solar Energy," Freiburg, Germany, Sep. 16, 2019. [Online]. Available: <https://www.ise.fraunhofer.de/en/publications/studies/photovoltaics-report.html>
- [2] A. Richter, M. Hermle, and S. W. Glunz, "Reassessment of the limiting efficiency for crystalline silicon solar cells," *IEEE J. Photovolt.*, vol. 3, no. 4, pp. 1184–1191, Oct. 2013.
- [3] "International technology roadmap for photovoltaic (ITRPV)," 2019. [Online]. Available: <http://www.itrpv.net/Reports/Downloads/>
- [4] T. Matsui *et al.*, "Development of highly stable and efficient amorphous silicon based solar cells," in *Proc. 28th Eur. Photovolt. Sol. Energy Conf. Exhib.*, 2013, pp. 2213–2217.
- [5] J. P. Mailoa *et al.*, "A 2-terminal perovskite/silicon multijunction solar cell enabled by a silicon tunnel junction," *Appl. Phys. Lett.*, vol. 106, no. 12, 2015, Art. no. 121105.
- [6] S. Essig *et al.*, "Realization of GaInP/Si dual-junction solar cells with 29.8% 1-Sun efficiency," *IEEE J. Photovolt.*, vol. 6, no. 4, pp. 1012–1019, Jul. 2016.
- [7] J. V. Holm *et al.*, "Bandgap optimized III-V (GaAsP) nanowire on silicon tandem solar cell, device and data," in *Proc. IEEE 40th Photovolt. Spec. Conf.*, Denver, CO, USA, 2014, pp. 1041–1044.
- [8] T. J. Grassman, J. A. Carlin, C. Ratcliff, D. J. Chmielewski, and S. A. Ringel, "Epitaxially-grown metamorphic GaAsP/Si dual-junction solar cells," in *Proc. IEEE 39th Photovolt. Spec. Conf.*, Tampa, FL, USA, 2013, pp. 149–153.
- [9] R. Gottschalg, D. G. Infield, and M. J. Kearney, "Experimental study of variations of the solar spectrum of relevance to thin film solar cells," *Sol. Energy Mater. Sol. Cells*, vol. 79, no. 4, pp. 527–537, 2003.
- [10] G. Nofuentes, B. García-Domingo, J. V. Muñoz, and F. Chenlo, "Analysis of the dependence of the spectral factor of some PV technologies on the solar spectrum distribution," *Appl. Energy*, vol. 113, pp. 302–309, 2014.
- [11] J. Y. Ye, T. Reindl, A. G. Aberle, and T. M. Walsh, "Effect of solar spectrum on the performance of various thin-film PV module technologies in tropical singapore," *IEEE J. Photovolt.*, vol. 4, no. 5, pp. 1268–1274, Sep. 2014.
- [12] P. Faine, S. R. Kurtz, C. Riordan, and J. M. Olson, "The influence of spectral solar irradiance variations on the performance of selected single-junction and multijunction solar cells," *Sol. Cells*, vol. 31, no. 3, pp. 259–278, 1991.
- [13] M. Morales-Masis, S. de Wolf, R. Woods-Robinson, J. W. Ager, and C. Ballif, "Transparent electrodes for efficient optoelectronics," *Adv. Electron. Mater.*, vol. 3, no. 5, 2017, Art. no. 1600529. [Online]. Available: <https://escholarship.org/content/qt52n985kq/qt52n985kq.pdf>

- [14] O. Dupré, B. Niesen, S. de Wolf, and C. Ballif, "Field performance versus standard test condition efficiency of tandem solar cells and the singular case of perovskites/silicon devices," *J. Phys. Chem. Lett.*, vol. 9, pp. 446–458, 2018. [Online]. Available: <http://pubs.acs.org/doi/pdf/10.1021/acs.jpclett.7b02277>
- [15] I. M. Peters, H. Liu, T. Reindl, and T. Buonassisi, "Global prediction of photovoltaic field performance differences using open-source satellite data," *Joule*, vol. 2, no. 2, pp. 307–322, 2018.
- [16] J. Lehr *et al.*, "Energy yield modelling of perovskite/silicon two-terminal tandem PV modules with flat and textured interfaces," *Sustain. Energy Fuels*, vol. 8, p. 506, 2018.
- [17] M. T. Hörantner and H. J. Snaith, "Predicting and optimising the energy yield of perovskite-on-silicon tandem solar cells under real world conditions," *Energy Environ. Sci.*, vol. 10, no. 9, pp. 1983–1993, 2017.
- [18] M. Jošt *et al.*, "Textured interfaces in monolithic perovskite/silicon tandem solar cells: Advanced light management for improved efficiency and energy yield," *Energy Environ. Sci.*, vol. 11, no. 12, pp. 3511–3523, 2019.
- [19] M. Steiner, G. Siefert, T. Hornung, G. Peharz, and A. W. Bett, "YieldOpt, a model to predict the power output and energy yield for concentrating photovoltaic modules," *Prog. Photovolt., Res. Appl.*, vol. 23, no. 3, pp. 385–397, 2015.
- [20] H. Schulte-Huxel, T. J. Silverman, M. G. Deceglie, D. J. Friedman, and A. C. Tamboli, "Energy yield analysis of multiterminal Si-based tandem solar cells," *IEEE J. Photovolt.*, vol. 8, no. 5, pp. 1376–1383, Sep. 2018.
- [21] R. Schmager *et al.*, "Methodology of energy yield modelling of perovskite-based multi-junction photovoltaics," *Opt. Express*, vol. 27, no. 8, 2019, Art. no. A507.
- [22] N. Tucher *et al.*, "Energy yield analysis of textured perovskite silicon tandem solar cells and modules," *Opt. Express*, vol. 27, no. 20, 2019, Art. no. A1419.
- [23] E. F. Fernández, D. L. Talavera, F. M. Almonacid, and G. P. Smestad, "Investigating the impact of weather variables on the energy yield and cost of energy of grid-connected solar concentrator systems," *Energy*, vol. 106, pp. 790–801, 2016.
- [24] D. Dimberger, G. Blackburn, B. Müller, and C. Reise, "On the impact of solar spectral irradiance on the yield of different PV technologies," *Sol. Energy Mater. Sol. Cells*, vol. 132, pp. 431–442, 2015.
- [25] Y. Boose, C. Heller, O. Stern, and M. Lynass, "The effect of spectral mismatch on the annual energy output of CdTe-, CIGS- and Si-based photovoltaic modules," in *Proc. 27th Eur. Photovolt. Sol. Energy Conf. Exhib.*, 2012, pp. 3194–3198.
- [26] M. Alonso-Abella, F. Chenlo, G. Nofuentes, and M. Torres-Ramírez, "Analysis of spectral effects on the energy yield of different PV (photovoltaic) technologies: The case of four specific sites," *Energy*, vol. 67, pp. 435–443, 2014.
- [27] H. Liu *et al.*, "The realistic energy yield potential of GaAs-on-Si tandem solar cells: A theoretical case study," *Opt. Express*, vol. 23, no. 7, 2015, Art. no. A382.
- [28] Y. Xie and M. Sengupta, "A fast All-sky radiation model for solar applications with narrowband irradiances on tilted surfaces (FARMS-NIT): Part I. The clear-sky model," *Sol. Energy*, vol. 174, pp. 691–702, 2018.
- [29] Y. Xie, M. Sengupta, and C. Wang, "A fast All-sky radiation model for solar applications with narrowband irradiances on tilted surfaces (FARMS-NIT): Part II. The cloudy-sky model," *Sol. Energy*, vol. 188, pp. 799–812, 2019.
- [30] J. C. M. Perez, "Impact of outdoor conditions to the power generation of silicon based tandem solar cells," Master's thesis, Albert-Ludwigs-Univ. of Freiburg, Freiburg, Germany, 2019.
- [31] R. Mueller, T. Behrendt, A. Hammer, and A. Kemper, "A new algorithm for the satellite-based retrieval of solar surface irradiance in spectral bands," *Remote Sens.*, vol. 4, no. 3, pp. 622–647, 2012.
- [32] A. Amillo, T. Huld, P. Vourlioti, R. Müller, and M. Norton, "Application of satellite-based spectrally-resolved solar radiation data to PV performance studies," *Energies*, vol. 8, no. 5, pp. 3455–3488, 2015.
- [33] T. Behrendt *et al.*, "Solar spectral irradiance derived from satellite data: A tool to improve thin film PV performance estimations?," *Sol. Energy*, vol. 98, pp. 100–110, 2013.
- [34] S. Kato, T. P. Ackerman, J. H. Mather, and E. E. Clothiaux, "The k-distribution method and correlated-k approximation for a shortwave radiative transfer model," *J. Quantitative Spectrosc. Radiative Transfer*, vol. 62, no. 1, pp. 109–121, 1999. [Online]. Available: <http://www.sciencedirect.com/science/article/pii/S0022407398000752>
- [35] T. Stoffel and A. Andreas, "NREL solar radiation research laboratory (SRRL): Baseline measurement system (BMS); Golden, Colorado (Data)," NREL, Golden, CO, USA, NREL Rep. DA-5500-56488, 1981, doi: [10.5439/1052221](https://doi.org/10.5439/1052221).
- [36] W. W. Nyamsi, B. Espinar, P. Blanc, and L. Wald, "How close to detailed spectral calculations is the k-distribution method and correlated-k approximation of Kato *et al.* (1999) in each spectral interval?," *Metz*, vol. 23, no. 5, pp. 547–556, 2014.
- [37] W. W. Nyamsi *et al.*, "A new method for estimating UV fluxes at ground level in cloud-free conditions," *Atmos. Meas. Tech. Discuss.*, vol. 10, pp. 4965–4978, 2017, doi: [10.5194/amt-10-4965-2017](https://doi.org/10.5194/amt-10-4965-2017).
- [38] F. Oviedo *et al.*, "Ohmic shunts in two-terminal dual-junction solar cells with current mismatch," *Jpn. J. Appl. Phys.*, vol. 56, no. 8S2, 2017, Art. no. 08MA05.
- [39] C. Sah, R. Noyce, and W. Shockley, "Carrier generation and recombination in P-N junctions and P-N junction characteristics," in *Proc. IRE*, vol. 45, no. 9, pp. 1228–1243, 1957.
- [40] P. Singh, S. Singh, M. Lal, and M. Husain, "Temperature dependence of I-V characteristics and performance parameters of silicon solar cell," *EuroSun2004*, vol. 92, no. 12, pp. 1611–1616, 2008.
- [41] M. W. Wanlass *et al.*, "Practical considerations in tandem cell modeling," *Sol. Cells*, vol. 27, no. 1/4, pp. 191–204, 1989.
- [42] O. Höhn, A. W. Walker, A. W. Bett, and H. Helmers, "Optimal laser wavelength for efficient laser power converter operation over temperature," *Appl. Phys. Lett.*, vol. 108, no. 24, 2016, Art. no. 241104.
- [43] W. Shockley and H. J. Queisser, "Detailed balance limit of efficiency of p-n junction solar cells," *J. Appl. Phys.*, vol. 32, no. 3, 1961, Art. no. 510.
- [44] J. Beier and B. Voss, "Humps in dark I-V-curves-analysis and explanation," in *Proc. 23rd IEEE Photovolt. Spec. Conf.*, Louisville, KY, USA, 1993, pp. 321–326.
- [45] I. Vurgaftman, J. R. Meyer, and L. R. Ram-Mohan, "Band parameters for III-V compound semiconductors and their alloys," *J. Appl. Phys.*, vol. 89, no. 11, 2001, Art. no. 5815.
- [46] Y. P. Varshni, "Temperature dependence of the energy gap in semiconductors," *Physica*, vol. 34, no. 1, pp. 149–154, 1967.
- [47] A. W. Walker, J. F. Wheeldon, O. Theriault, M. D. Yandt, and K. Hinzer, "Temperature dependent external quantum efficiency simulations and experimental measurement of lattice matched quantum dot enhanced multi-junction solar cells," in *Proc. 37th IEEE Photovolt. Spec. Conf.*, Seattle, WA, USA, 2011, pp. 564–569.
- [48] A. Richter *et al.*, "n-type Si solar cells with passivating electron contact: Identifying sources for efficiency limitations by wafer thickness and resistivity variation," *Sol. Energy Mater. Sol. Cells*, vol. 173, pp. 96–105, 2017.
- [49] C. L. Schilling *et al.*, "Combining photon recycling and concentrated illumination in a GaAs heterojunction solar cell," *IEEE J. Photovolt.*, vol. 8, no. 1, pp. 348–354, Jan. 2018.
- [50] N. Tucher *et al.*, "Optical simulation of photovoltaic modules with multiple textured interfaces using the matrix-based formalism OPTOS," *Opt. Express*, vol. 24, no. 14, pp. A1083–A1093, 2016.
- [51] N. Tucher, "Analysis of photonic structures for silicon solar cells," Ph.D. dissertation, IMTEK, Albert-Ludwigs-Universität, Freiburg, Germany, 2016.
- [52] J. N. Murthy, "The role of irradiance spectra for yield analyses of tandem solar cells," Master's thesis, Fraunhofer-ISE, Albert-Ludwigs-Universität, Freiburg, Germany, 2019.
- [53] D. Dimberger, B. Müller, and C. Reise, "PV module energy rating: Opportunities and limitations," *Prog. Photovolt., Res. Appl.*, vol. 23, no. 12, pp. 1754–1770, 2015.
- [54] C. M. Fernández-Peruchena, M. Blanco, M. Gastón, and A. Bernardos, "Increasing the temporal resolution of direct normal solar irradiance series in different climatic zones," *Sol. Energy*, vol. 115, pp. 255–263, 2015.
- [55] M. Ernst and J. Gooday, "Methodology for generating high time resolution typical meteorological year data for accurate photovoltaic energy yield modelling," *Sol. Energy*, vol. 189, pp. 299–306, 2019.
- [56] J. Polo, L. F. Zarzalejo, R. Marchante, and A. A. Navarro, "A simple approach to the synthetic generation of solar irradiance time series with high temporal resolution," *Sol. Energy*, vol. 85, no. 5, pp. 1164–1170, 2011.